**Climate
of the Past**
Open Access
Discussions

Natural periodicities and north–south hemispheres connection of fast temperature changes during the last glacial period: EPICA and NGRIP revisited

T. Alberti[1], F. Lepreti[1,2], A. Vecchio[3,1], E. Bevacqua[1], V. Capparelli[1], and V. Carbone[1,4]

[1]Dipartimento di Fisica, Università della Calabria, Ponte P. Bucci 31C, 87036 Rende (CS), Italy
[2]CNISM Unità di Cosenza, Ponte P. Bucci 31C, 87036 Rende (CS), Italy
[3]Istituto Nazionale di Geofisica e Vulcanologia, Sede di Cosenza, Rende (CS), Italy
[4]CNR-ISAC, Lamezia Terme (CZ), Italy

Correspondence to: F. Lepreti (fabio.lepreti@fis.unical.it)

Discussion Paper | Discussion Paper | Discussion Paper | Discussion Paper |

CPD

10, 1129–1152, 2014

Fast temperature changes during the last glacial period

T. Alberti et al.

Title Page

Abstract | Introduction

Conclusions | References

Tables | Figures

|◄ | ►|

◄ | ►

Back | Close

Full Screen / Esc

Printer-friendly Version

Interactive Discussion

Abstract

We investigate both the European Project for Ice Coring in Antarctica (EPICA) and North Greenland Ice-Core Project (NGRIP) datasets to study the time evolution of the so-called Dansgaard–Oeschger events during the last glacial period. The Empirical Mode Decomposition (EMD) is used to extract the proper modes of both the datasets. It is shown that the time behaviour of Dansgaard–Oeschger events is captured by three EMD modes, while three more EMD modes can be used to describe the evolution at longer time scales. Using EMD signal reconstructions and a simple model based on the one-dimensional Langevin equations, it is argued that the occurrence of a Dansgaard–Oeschger event can be described as an excitation of the climate system within the same state, while the longer time scale behaviour appears to be due to transitions between different states. Finally, on the basis of a cross-correlation analysis performed on EMD reconstructions, evidence is presented that the Antarctic climate changes lead that of Greenland by a lag of ≈ 3.6 kyr.

1 Introduction

Some time ago, it has been suggested that the climate of the Holocene period is much more variable than believed, being perhaps part of a millennial-scale pattern (Denton and Karlén, 1973; O'Brien et al., 1995; Bond et al., 1997). Oxygen isotope $\delta^{18}O$ data from Greenland ice cores (North Greenland Ice Core Project members, 2004) reveal that the sub-Milankovitch climate variability presents abrupt temperature fluctuations which dominated the climate in Greenland between 11 and 74 thousand years before present (kyr B.P.). These fluctuations, known as Dansgaard–Oeschger (DO) events, are characterized by fast warmings and slow coolings, with temperature increasing up to 15 °C compared to glacial values. Less pronounced recurrent events, known as Antarctic Isotope Maxima (AIM), have been recognized over the same period in

Antarctic, even if they are characterized by rather gradual warming and cooling (EPICA-members, 2004).

The claimed roughly periodic, non-sinusoidal character of these events, with a basic period of about $T \simeq 1450$–1500 yr, has been questioned on the basis of the fact that a null random hypothesis for these events cannot be fully rejected (Ditlevsen et al., 2007; Schulz, 2002; Peavoy and Franzke, 2010). This is obviously due to the fact that the criteria used for a definition of DO events cannot be firmly established. The usual numbered DO events were firstly determined visually (Dansgaard et al., 1993), but when different definitions are used, some events are excluded from the list or additional events are included, thus changing the basic periodicity (Ditlevsen et al., 2007; Schulz, 2002; Rahmstorf, 2003; Alley et al., 2001; Ditlevsen et al., 2005; Bond et al., 1999). For example, Schulz (2002) showed that the basic cycle is determined solely by DO events 5, 6, and 7, even if a fundamental period of about 1470 years seems to control the timing of the onset of the events. On the other hand, different periodicities in the range $1 \div 2$ kyr have been found from deep-sea sediment cores in the sub-polar North Atlantic (Bond et al., 1999). Of course, the main problem comes from the non-stationarity of the oxygen isotope dataset (Ditlevsen et al., 2007; Schulz, 2002).

DO events are widely described through models involving coupling between the Atlantic ocean thermohaline circulation and changes in atmospheric circulation and sea-ice cover (e.g. Rahmstorf, 2003). In particular, ice volume plays a relevant role in affecting the ocean–atmosphere system, as suggested by the fact that the Holocene interglacial period has not shown the extreme DO variability typical of the last ice age.

In this paper, we present a study of DO events in the two hemispheres, based on the analysis of the European Project for Ice Coring in Antarctica and North Greenland Ice–Core Project datasets. The Empirical Mode Decomposition technique is used to identify and characterize observed climate variability on different time scales.

Title Page

Abstract | Introduction

Conclusions | References

Tables | Figures

|◄ | ►|

◄ | ►

Back | Close

Full Screen / Esc

Printer-friendly Version

Interactive Discussion

2 Datasets and analysis technique

The European Project for Ice Coring in Antarctica (EPICA) dataset provides a record of 100 yr averages of the oxygen isotope δ^{18}O from the EPICA Dronning Maud Land Ice Core (75.00° S, 0.07° E, 2892 metres a.s.l.) covering the period 10÷51 kyr B.P. (EPICA-members, 2006). Data for the Northern Hemisphere come from the North Greenland Ice–Core Project (NGRIP, 75.10° N, 42.32° W, 2917 m elevation) and consist in 50 yr averages of δ^{18}O extending back to 123 kyr B.P. (North Greenland Ice Core Project members, 2004). We consider here the period 20 ÷ 43.5 kyr B.P. for both the datasets (see Fig. 1).

2.1 The Empirical Mode Decomposition

To identify the main periodicities and their amplitudes, we applied the Empirical Mode Decomposition (EMD), a technique designed to investigate non-stationary data (Huang et al., 1998). The EMD has been extensively and successfully used in different fields (Cummings et al., 2004; Terradas et al., 2004; Franzke, 2009; Vecchio et al., 2010a, b; Capparelli et al., 2011; Vecchio et al., 2012). Both the δ^{18}O time series are decomposed, by means of the EMD, into a finite number m of oscillating intrinsic mode functions (IMFs) as

$$\delta^{18}O = \sum_{j=0}^{m-1} C_j(t) + r_m(t). \tag{1}$$

The functional form of the IMFs, $C_j(t)$, is not given a priori, but obtained from the data through the algorithm developed by Huang et al. (1998). As a first step, the local extrema, minima and maxima, are identified in the raw data δ^{18}O. The local extrema are interpolated by means of cubic splines to obtain the envelopes of the maxima and minima. Then the difference $h_1(t)$ between δ^{18}O and $m_1(t)$, the latter being the mean between the envelopes of the maxima and minima, is computed. If this quantity

Full Screen / Esc

Printer-friendly Version

Interactive Discussion

satisfies the following two conditions, (i) the number of extrema and zero crossings does not differ by more than 1 and (ii) the mean value of the envelopes obtained from the local maxima and minima is zero at any point, it represents an IMF. If the conditions above are not fulfilled, the described procedure is repeated on the $h_1(t)$ time series, and $h_{11}(t) = h_1(t) - m_{11}(t)$, where $m_{11}(t)$ is the mean of the new envelopes, is calculated. This process is iterated until, after s times, $h_{1s}(t)$ fulfils the IMF properties. To avoid a loss of information about amplitude and frequency modulations, a criterion to stop the above described procedure has been proposed (Huang et al., 1998) by defining

$$\sigma = \sum_{t=0}^{N} \left[\frac{|h_{1(s-1)}(t) - h_{1s}(t)|^2}{h_{1(s-1)}^2(t)} \right], \tag{2}$$

calculated between two consecutive iterations. The iterations are stopped when σ is smaller than a threshold σ_{th}, which is typically fixed at $\simeq 0.3$ (Huang et al., 1998). When the first IMF $C_1(t)$ is obtained, the "first residue" $r_1(t) = \delta^{18}O - C_1(t)$ is calculated and processed in the same way as previously explained. A new IMF $C_2(t)$ and a second residue $r_2(t)$ are then obtained. This procedure is carried on until C_s or r_s are almost constant or when the residue $r_s(t)$ is monotonic. As a result of this method, the original signal is decomposed into m empirical modes, ordered in increasing characteristic time scale, and a residue $r_m(t)$ which provides the mean trend, if any exists in the dataset. Each $C_j(t)$ represents a zero mean oscillation $C_j(t) = A(t)\sin\phi(t)$ (being $\phi(t)$ the instantaneous phase) experiencing modulation both in amplitude $A(t)$ and frequency $\omega = d\phi/dt$. A typical average period T_j can be estimated for all the IMFs. Since the decomposition is local, complete, and orthogonal, the EMD can be used as a filter by reconstructing the signal through partial sums in Eq. (1) (Huang et al., 1998; Cummings et al., 2004; Vecchio et al., 2010a).

The statistical significance of the IMFs with respect to a white noise has been verified through the test developed by Wu and Huang (2004). This is based on the constancy of the product between the mean square amplitude of each IMF and the corresponding

average period when the EMD is applied to a white noise series. This allows to derive, for each IMF, the analytical mean square amplitude spread function for different confidence levels. Therefore, by comparing the mean square amplitude of the EMD modes obtained from the data under analysis to the theoretical spread function, the IMFs containing information at a given confidence level can be discerned from purely noisy IMFs.

3 Empirical Mode Decomposition results

Applying the EMD procedure to the EPICA and NGRIP data, we obtain a set of $m = 6$ IMFs for EPICA (see Fig. 2), which we denote as $C_j^{(S)}(t)$, and $m = 7$ IMFs, named $C_j^{(N)}(t)$, for NGRIP (see Fig. 3). We remark that while $r_m(t)$ for the NGRIP dataset represents a real monotonic trend, for the EPICA sample it consists of an oscillating function with an offset representing the mean value of the δ^{18}O proxy. Therefore, for EPICA we will consider $r_m(t)$, after subtracting its temporal mean $\langle r_m(t) \rangle$, as a genuine IMF.

The results of the significance test are shown in Fig. 4. In performing the test, it was assumed that the energy of the IMFs $j = 0$ comes only from noise and it is thus assigned to the 99 % line. The modes which are above the spread line can be considered significant at 99th percentile. For EPICA the modes $j = 2$–5 are significant, while the mode $j = 1$ lies just on the spread line. For NGRIP all the modes $j = 1$–6 result to be significant.

Performing the Hilbert transform of each IMF

$$C_j^*(t) = \frac{1}{\pi} P \int_{-\infty}^{\infty} \frac{C_j(t')}{t - t'} dt', \tag{3}$$

Fast temperature changes during the last glacial period

T. Alberti et al.

where P denotes the Cauchy principal value and $C_j^*(t)$ is the complex conjugate of $C_j(t)$, the instantaneous phase can be calculated as $\phi(t) = \arctan[C_j^*(t)/C_j(t)]$ and the instantaneous frequency $\omega_j(t)$ and period $T_j(t)$ are given by $\omega_j(t) = 2\pi/T_j(t) = d\phi_j/dt$. The characteristic periods $\bar{T}_j$ are estimated as the time averages of $T_j(t)$ and reported in Table 1.

More than one IMF is needed to reproduce the observed DO events. In fact, the main DO events are captured by the sum of the $j = 1, 2, 3$ modes, as shown in Fig. 5 where we report the superposition of the raw δ^{18}O data for both the EPICA and NGRIP datasets, and the two reconstructions given by

$$N_H(t) = \sum_{j=1,3} C_j^{(N)}(t), \tag{4}$$

$$S_H(t) = \sum_{j=1,3} C_j^{(S)}(t). \tag{5}$$

In order to investigate the variability at longer time scales with respect to those involved in DO events, we can consider the IMFs $j = 4, 5, 6$. Long term reconstructions, defined as,

$$N_L(t) = \sum_{j=4,6} C_j^{(N)}(t) \tag{6}$$

$$S_L(t) = \sum_{j=4,5} C_j^{(S)}(t) + (r_n(t) - \langle r_n(t) \rangle) \tag{7}$$

are reported as blue lines in Fig. 5. Reconstructions with long period IMFs $j = 4$–6 underline the long term trend, characterized by intervals in which DO events happen and intervals when these are not observed.

The results of the EMD decomposition suggest that the evolution of cooling-warming cycles over the investigated period can be described in terms of two dynamical processes occurring on different time-scales. A simple model of such a phenomenology is considered in the next section.

Fast temperature changes during the last glacial period

T. Alberti et al.

Title Page

Abstract | Introduction

Conclusions | References

Tables | Figures

◄ | ►

◄ | ►

Back | Close

Full Screen / Esc

Printer-friendly Version

Interactive Discussion

4 Potential analysis

Glacial-interglacial cycles are commonly modelled as transitions between different climate states (see e.g. Paillard, 2001). The same approach has been extended to DO events that are commonly modelled as a two-state, cold/stadial and warm/interstadial, system. In the following we apply the method developed by Livina et al. (2010) to identify the number of climate states present in both NGRIP and EPICA records. To this purpose, the climate system is described in term of a nonlinear system with many dynamical states and we assume that transitions among states are triggered by a stochastic forcing. A very simple model for this is the one-dimensional Langevin equation (Livina et al., 2010):

$$\mathrm{d}z = -U(z)\mathrm{d}t + \sigma\mathrm{d}W \tag{8}$$

where z represents, in our case, the oxygen isotope $\delta^{18}O$, $U(z)$ is the potential, σ is the noise level and W is a Wiener process. A stationary solution of Eq. (8) is found when $U(z)$ is a polynomial of even order and positive leading coefficient. The order of the polynomial fixes the number of available states: for example, a second order polynomial corresponds to a system with single-well potential and one state, while a fourth-order polynomial, corresponding to a double-well potential, identifies a system with two states. The number of states can be evaluated from the data by performing a polynomial fit of the probability density function (pdf) calculated as

$$p(z) \sim \exp[-2U(z)/\sigma^2] \tag{9}$$

representing a stationary solution of the Fokker–Planck equation

$$\frac{\partial p(z,t)}{\partial t} = \frac{\partial[U(z)p(z,t)]}{\partial z} + \frac{1}{2}\sigma^2\frac{\partial^2 p(z,t)}{\partial z^2}. \tag{10}$$

Equation (9) establishes a one to one correspondence between the potential and the the pdf of the system so that

$$U(z) = -\frac{\sigma^2}{2} \ln p_{emp}(z) , \tag{11}$$

where $p_{emp}(z)$ is the empirical pdf extracted from data. To estimate $p_{emp}(z)$ we used the Kernel Density estimator (Silverman, 1998; Hall, 1992)

$$\hat{f}(z) = \frac{1}{nh} \sum_{i=1}^{n} K\left(\frac{z - z_i}{h}\right) , \tag{12}$$

where K is the kernel, a symmetric function that integrates to one, z_i are the data points, and $h > 0$ is a smoothing parameter denoted as bandwidth. The corresponding variance is:

$$\hat{\sigma}(z) = \frac{1}{nh} \left[\frac{1}{nh} \sum_{i=1}^{n} K\left(\frac{z - z_i}{h}\right)^2 - h\hat{f}(z)^2 \right] . \tag{13}$$

For the following application we use the Epanechnikov kernel, which is optimal in a minimum variance sense and we chose $h = 0.9 * s/n^{0.2}$, where s is the standard deviation of the data set. The confidence interval of $\hat{f}(z)$ has been evaluated through a bootstrap. Being

$$\hat{f}^*(z) = \frac{1}{nh^*} \sum_{i=1}^{n} K\left(\frac{z - z_i^*}{h^*}\right) \tag{14}$$

the bootstrap estimator of $p_{emp}(z)$,

$$\hat{\sigma}^*(z) = \frac{1}{nh^*} \left[\frac{1}{nh^*} \sum_{i=1}^{n} K\left(\frac{z - z_i^*}{h^*}\right)^2 - h^*\hat{f}(z)^2 \right] \tag{15}$$

Title Page

Abstract | Introduction

Conclusions | References

Tables | Figures

◀ | ▶

◀ | ▶

Back | Close

Full Screen / Esc

Printer-friendly Version

Interactive Discussion

the variance of $\hat{f}^*(z)$ and

$$\hat{t}^*(z) = \frac{\hat{f}^*(z) - \hat{f}(z)}{\hat{\sigma}^*(z)} \tag{16}$$

the bootstrap t-statistic (Hall, 1992), the symmetric confidence interval with coverage probability $1 - \alpha$ is $[\hat{f}(z) - \hat{\sigma}(z)u^*_{1-\alpha/2}, \hat{f}(z) - \hat{\sigma}(z)u^*_{\alpha/2}]$ where $u^*_{\alpha/2}$ is the bootstrap estimate of the quantile defined by $P(\hat{t}^*(z) \leq u^*_{\alpha/2}) = \alpha/2$ and $u^*_{1-\alpha/2}$ is the bootstrap estimate of the quantile defined by $P(\hat{t}^*(z) \leq u^*_{1-\alpha/2}) = 1 - \alpha/2$ (Hall, 1992). In order to remove asymptotic biases which are not correctly taken into account by the bootstrap procedure, we perform an under-smoothing by choosing a smaller bandwidth $h^* = 0.9 * s/n^{0.25} < h$ (Hall, 1992). This procedure allows to calculate $U(z)$ with the corresponding uncertainty from Eq. (11).

In order to investigate the time evolution of the DO events, potentials have been separately calculated for $N_H(t)$, $S_H(t)$ and $N_L(t)$, $S_L(t)$ and reported in Fig. 6. The potentials associated with $N_H(t)$, $S_H(t)$ and the corresponding best fits are shown in panels a and b respectively. The best fit polynomials are of 2nd order, thus corresponding to a single well potential. Therefore, the occurrence of a DO event could not be due to a transition of the system to a different dynamical state but to an excitation of the system within the same state. On the other hand, the $U(z)$ calculated for $N_L(t)$, $S_L(t)$ are well fitted by 4th order polynomials, indicating the occurrence of a double-well potential, thus suggesting that the high activity, when the DO events are observed, and low activity periods correspond to different states of the climatic system.

5 The north–south asyncrony

An important aspect of the polar climate dynamics is the understanding of how Earth's hemispheres have been coupled during past climate changes. Bender et al. (1994)

explored the possible connections between Greenland and Antarctica climate, suggesting that partial deglaciation and changes in ocean circulation are the main mechanisms which transfer warmings in Northern Hemisphere climate to Antarctica. Different analyses showed that southern changes are not a direct response to abrupt changes in North Atlantic thermohaline circulation, as is assumed in the conventional picture of a hemispheric temperature seesaw (Morgan et al., 2002). The study of the global concentration of methane recorded in ice cores allowed to infer that Antarctic climate changes lead that of Greenland by $1 \div 2.5$ kyr over the period 47–23 kyr before present (Blunier et al., 1998).

In order to investigate this issue, we study the cross-correlation between the EPICA and NGRIP reconstructions obtained from the EMD as illustrated in Sect. 3. The cross-correlation coefficient $P_{yz}(\Delta)$ between two time samples $y(t_k)$ and $z(t_k)$ is defined as

$$P_{yz}(\Delta) = \frac{\sum [y(t_k + \Delta) - \langle y \rangle][z(t_k) - \langle z \rangle]}{\sqrt{\sum [y(t_k) - \langle y \rangle]^2 \sum [z(t_k) - \langle z \rangle]^2}} \tag{17}$$

where brackets denote time averages and Δ the time lag. We calculated the cross-correlation coefficient both for the short time-scale reconstructions Eqs. (4) and (5) and for the long time-scale ones Eqs. (6) and (7). The two coefficients $P_{N_H S_H}(\Delta)$ and $P_{N_L S_L}(\Delta)$ are shown in Fig. 7. $P_{N_H S_H}(\Delta)$ displays oscillations with many peaks of similar amplitude at both negative and positive lags. This behaviour is typically obtained when oscillating signals having nearly the same frequency are compared. In this case, it is not possible to identify the leading and the following process. On the other hand, a peak which is significantly higher than the others, with a maximum value of ≈ 0.66, is found in $P_{N_L S_L}(\Delta)$ at $\Delta \approx 3.6$ kyr. This result supports the view according to which the Antarctic climate changes actually lead that of Greenland, but on a longer time-scale than previously reported.

6 Conclusions

In the present paper we study both the EPICA and NGRIP datasets, in order to investigate their periodicities and the possible existence of synchronization of abrupt climate changes observed in the North and South hemispheres. Our results can be summarized as follows.

1. Proper EMD modes, significant with respect to a random null hypothesis, are present in both datasets, thus confirming that natural cycles of abrupt climate changes during the last glacial period exist and their occurrence cannot be due to random fluctuations in time.

2. Due to the non-stationarity of the process, the dynamics of DO events is captured by three EMD modes, $j = 1$–3 for both the datasets. Therefore, the signal reconstructions obtained by summing the modes $j = 1$–3 reproduce the variability at the typical time scales of DO events. On the other hand, the reconstructions with the modes $j = 4$–6 can be used to describe the climate evolution at longer time scales, characterized by intervals in which DO events happen and intervals when these are not observed.

3. By comparing the EMD signal reconstructions to the results of a simple model based on the one-dimensional Langevin equation, evidence is found that the occurrence of a DO event can be described as an excitation of the system within the same climate state, rather than a transition between different states. Conversely, the longer time scale dynamics appear to be due to transitions between different climate states.

4. On the base of a cross correlation analysis between the NGRIP and EPICA EMD reconstructions, performed to investigate the north–south asynchrony, it is found that the clearest correlation occurs between the long-scale reconstructions at a lag $\Delta \approx 3.6\,\mathrm{kyr}$, which supports the view according to which the Antarctic climate

changes lead that of Greenland, but on a longer time-scale than previously reported.

We plan to extend the study presented in this paper to other paleoclimate records, in order to investigate the role of other physical processes, such ocean–atmosphere interaction and solar irradiance variations, in the climate system evolution. Moreover, the results presented in this paper could be useful for the theoretical modelling of the climate evolution in polar regions, in order to characterise the processes involved at different time scales and the coupling between northern and Southern Hemispheres.

References

Alley, R. B., Anandakrishnan, S., and Jung, P.: Stochastic resonance in the North Atlantic, Paleoceanography, 16, 190–198, 2001. 1131

Andersen, K. K., Svensson, A., Johnsen, S. J., Rasmussen, S. O., Bigler, M., Röthlisberger, R., Ruth, U., Siggaard-Andersen, M.-L., Steffensen, J. P., Dahl-Jensen, D., Vinther, B. M., and Clausen, H. B.: The Greenland Ice Core Chronology 2005, 15–42 ka. Part 1: Constructing the time scale, Quaternary Sci. Rev., 25, 3246–3257, 2006.

Bender, M., Sowers, T., Dickson, M.-L., Orchardo, J., Grootes, P., Mayewski, P. A., and Meese, D. A.: Climate correlations between Greenland and Antarctica during the past 100,000 years, Nature, 372, 663–666, 1994. 1138

Blunier, T., Chappellaz, J., Schwander, J., Dällenbach, A., Stauffer, B., Stocker, T. F., Raynaud, D., Jouzer, J., Clausen, H. B., Hammer, C. U., and Johnsen, S. J.: Asyncrony of Antarctic and Greenland climate change during the last glacial period, Nature, 394, 739–743, 1998. 1139

Bond, G. C., Showers, W., Cheseby, M., Lotti, R., Almasi, P., de Menocal, P., Priore, P., Cullen, H., Hajdas, I., and Bonani, G.: A pervasive millennial-scale cycle in North Atlantic Holocene and glacial climates, Science, 278, 1257–1266, 1997. 1130

Bond, G. C., Showers, W., Elliot, M., Evans, M., Lotti, R., Hajdas, I., Bonani, G., and Johnson, S.: The North Atlantic's l-2 kyr climate rhythm: relation to Heinrich Events,

Dansgaard/Oeschger cycles and the Little Ice Age, Mechanisms of Global Climate Change at Millennial Time Scales, Geophysical Monograph 112 (AGU), 1999. 1131

Capparelli, V., Vecchio, A., and Carbone, V.: Long-range persistence of temperature records induced by long-term climatic phenomena, Phys. Rev. E, 84, 046103, doi:10.1103/PhysRevE.84.046103, 2011. 1132

Cummings, D. A. T., Irizarry, R. A., Huang, N. E., Endy, T. P., Nisalak, A., Ungchusak, K., and Burke, D. S.: Travelling waves in the occurrence of dengue haemorrhagic fever in Thailand, Nature, 427, 344–347, doi:10.1038/nature02225, 2004. 1132, 1133

Dansgaard, W., Johnsen, S. J., Clausen, H. B., Dahl-Jensen, D., Gundestrup, N. S., Hammer, C. U., Hvidberg, C. S., Steffensen, J. P., Sveinbjornsdottir, A. E., Jouzel, J., and Bond, G.: Evidence for general instability of past climate from a 250-kyr ice-core record, Nature, 364, 218–220, 1993. 1131

Denton, G. H. and Karlén, W.: Holocene climatic variations. Their pattern and possible cause, Quaternary Res., 3, 155–174, doi:10.1016/0033-5894(73)90040-9, 1973. 1130

Ditlevsen, P. D., Kristensen, M. S., and Andersen, K. K.: The recurrence time of Dansgaard-Oeschger events and limits on the possible periodic component, J. Climate, 18, 2594–2603, 2005. 1131

Ditlevsen, P. D., Andersen, K. K., and Svensson, A.: The DO-climate events are probably noise induced: statistical investigation of the claimed 1470 years cycle, Clim. Past, 3, 129–134, doi:10.5194/cp-3-129-2007, 2007. 1131

EPICA-members: Eight glacial cycles from Antarctic ice core, Nature, 429, 623–628, 2004. 1131

EPICA community members: One-to-one coupling of glacial climate variability in Greenland and Antarctica, Nature, 444, 195–198, 2006. 1132

Franzke, C.: Multi-scale analysis of teleconnection indices: climate noise and nonlinear trend analysis, Nonlinear Proc. Geoph., 16, 65–76, doi:10.5194/npg-16-65-2009, 2009. 1132

Hall, P.: Effect of bias estimation on coverage accuracy of bootstrap confidence intervals for a probability density, Ann. Stat., 20, 675–694, 1992. 1137, 1138

Huang, N. E., Shen, Z., Long, S. R., Wu, M. L. C., Shih, H. H., Zheng, Q. N., Yen, N. C., Tung, C. C., and Liu, H. H.: The empirical mode decomposition and the Hilbert spectrum for nonlinear and non-stationary time series analysis, P. Roy. Soc. Lond. A, 454, 903, 1998. 1132, 1133

Livina, V. N., Kwasniok, F., and Lenton, T. M.: Potential analysis reveals changing number of climate states during the last 60 kyr, Clim. Past, 6, 77–82, doi:10.5194/cp-6-77-2010, 2010. 1136

Morgan, V., Delmotte, M., van Ommen, T., Jouzel, J., Chappellaz, J., Woon, S., Masson-Delmotte, V., Raynaud, D.: Relative timing of deglacial climate events in Antarctica and Greenland, Science, 297, 1862–1864, 2002. 1139

North Greenland Ice Core Project members: High-resolution records of Northern Hemisphere climate extending into the last interglacial period, Nature, 431, 147–151, 2004. 1130, 1132

O'Brien, S. R., Mayewski, P. A., Meeker, L. D., Meese, D. A., Twickler, M. S., and Whitlow, S. I.: Complexity of Holocene Climate as Reconstructed from a Greenland Ice Core, Science, 270, 1962–1964, doi:10.1126/science.270.5244.1962, 1995. 1130

Paillard, D.: Glacial cycles: toward a new paradigm, Rev. Geophys., 39, 325–346, 2001. 1136

Peavoy, D. and Franzke, C.: Bayesian analysis of rapid climate change during the last glacial using Greenland δ^{18}O data, Clim. Past, 6, 787–794, doi:10.5194/cp-6-787-2010, 2010. 1131

Rahmstorf, S.: Timing of abrupt climate changes: A precise clock, Geophys. Res. Lett., 30, 1510–1514, 2003. 1131

Schulz, M.: On the 1470-year pacing of Dansgaard–Oeschger warm events, Paleoceanography, 17, 4, doi:10.1029/2000PA000571, 2002. 1131

Silverman, B. W.: Density estimation for statistics and data analysis, CRC Press, Boca Raton, 1998. 1137

Terradas, J., Oliver, R., and Ballester, J. L.: Application of statistical techniques to the analysis of solar coronal oscillations, Astrophys. J., 614, 435–447, doi:10.1086/423332 2004. 1132

Vecchio, A., Laurenza, M., Carbone, V., and Storini, M.: Quasi-biennial modulation of solar neutrino flux and solar and galactic cosmic rays by solar cyclic activity, Astrophys. J. Lett., 709, L1–L5, 2010a. 1132, 1133

Vecchio, A., Capparelli, V., and Carbone, V.: The complex dynamics of the seasonal component of USA's surface temperature, Atmos. Chem. Phys., 10, 9657–9665, doi:10.5194/acp-10-9657-2010, 2010b. 1132

Vecchio, A., D'Alessi, L., Carbone, V., Laurenza, M., and Storini, M.: The empirical mode decomposition to study the quasi-biennial modulation of solar magnetic activity and solar neutrino flux, Adv. Adapt. Data Anal., 04, 1250014, doi:10.1142/S1793536912500148, 2012. 1132

Wu, Z. and Huang, N. E.: A study of the characteristics of white noise using the empirical mode decomposition method, P. Roy. Soc. Lond. A, 460, 1597, 2004. 1133

Fast temperature changes during the last glacial period

T. Alberti et al.

Title Page

Abstract   Introduction

Conclusions   References

Tables   Figures

|◄   ►|

◄   ►

Back   Close

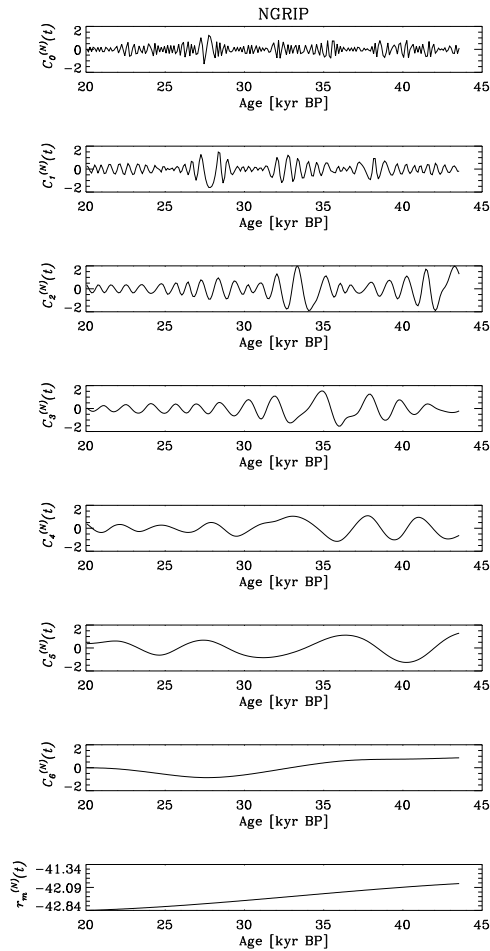Full Screen / Esc

Printer-friendly Version

Interactive Discussion

Table 1. Characteristic periods of both EPICA and NGRIP datasets obtained through the EMD. Errors are estimated as standard deviations of the instantaneous periods. The period of the $j = 6$ mode for EPICA refers to the residue $r_m(t)$ (see text).

j-th EMD mode	T_j (yr) EPICA	T_j (yr) NGRIP
1	540 ± 110	546 ± 170
2	1060 ± 250	1050 ± 250
3	2970 ± 680	1940 ± 600
4	5100 ± 1200	4000 ± 1400
5	9720 ± 930	7500 ± 2100
6	24800 ± 1400	24300 ± 3700

Full Screen / Esc

Printer-friendly Version

Interactive Discussion
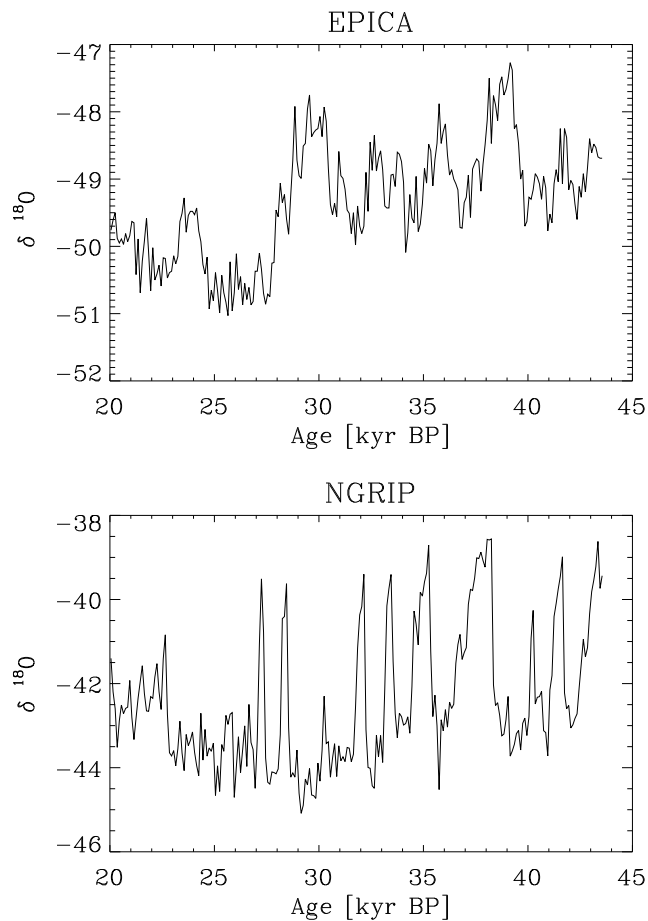
Fig. 1. δ^{18}O data for the EPICA (upper panel) and NGRIP (lower panel) datasets in the period $20 \div 43.5$ kyr B.P.
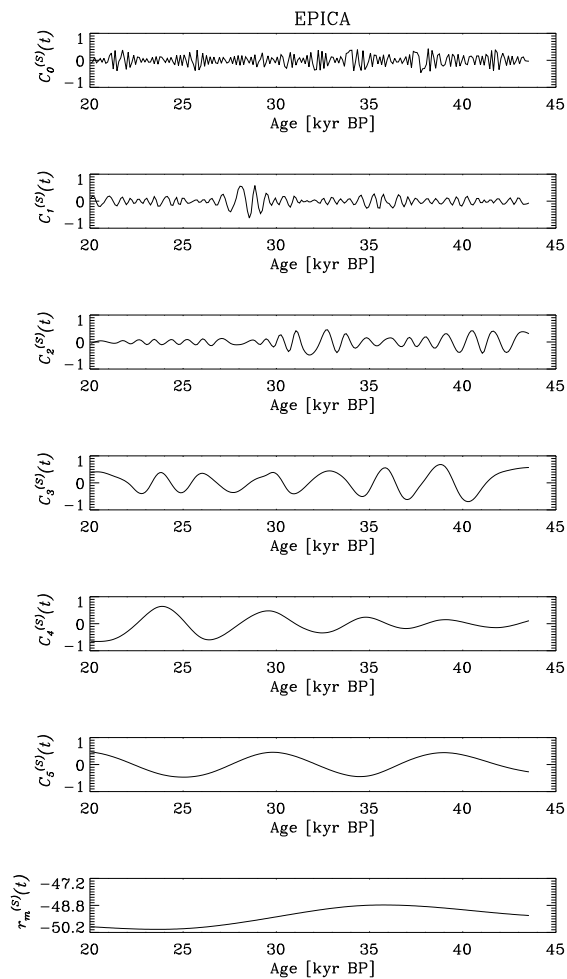
Fig. 2. IMFs $C_j^{(S)}(t)$ and residue $r_m^{(S)}(t)$ for the EPICA dataset.

Fig. 3. IMFs $C_j^{(N)}(t)$ and residue $r_m^{(N)}(t)$ for the NGRIP dataset.
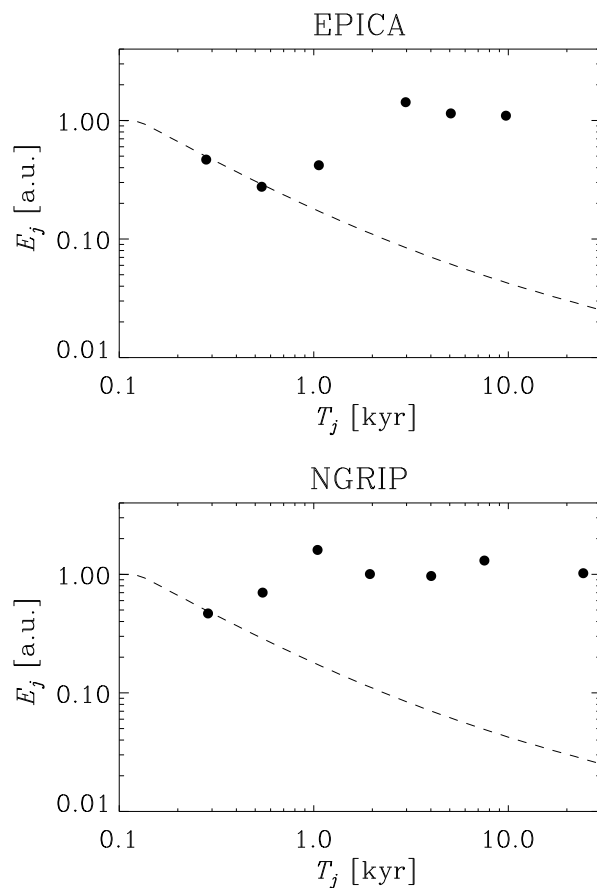
Fig. 4. Normalized IMF square amplitude E_j vs. the period T_j for the EMD significance test applied to the EPICA (upper panel) and NGRIP (lower panel) IMFs. The dashed lines represent the 99th percentile (see the text for details).

1149
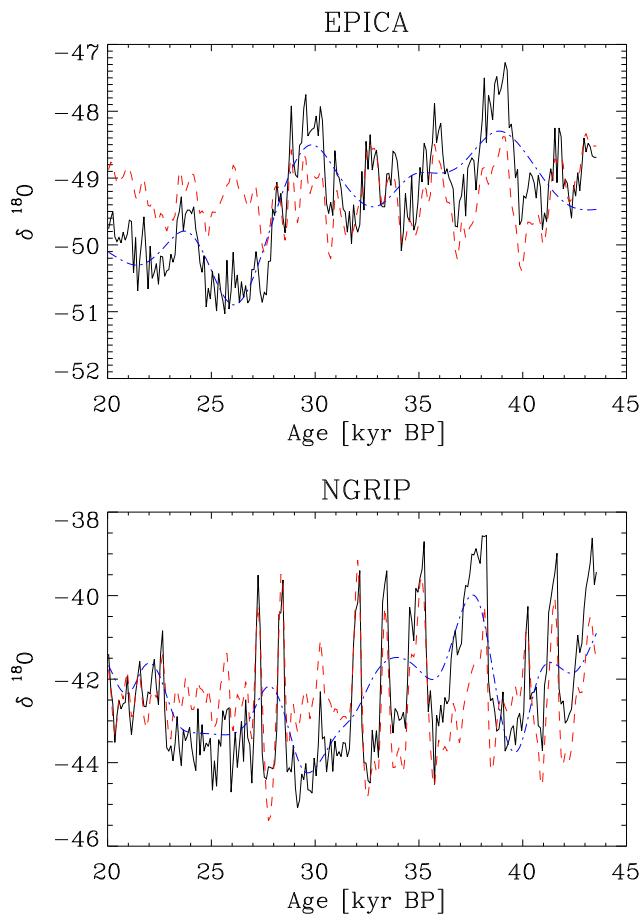
Fig. 5. δ^{18}O data (black solid lines), sums of the $j = 1, 2, 3$ IMFs (red dashed lines) and of the $j = 4, 5, 6$ modes (blue dash-dotted lines) for the EPICA (upper panel) and NGRIP (lower panel) datasets. An offset was applied to the IMF sums to allow visualization in the same plot.

Title Page

Abstract | Introduction

Conclusions | References

Tables | Figures

|◀ | ▶|

◀ | ▶

Back | Close

Full Screen / Esc

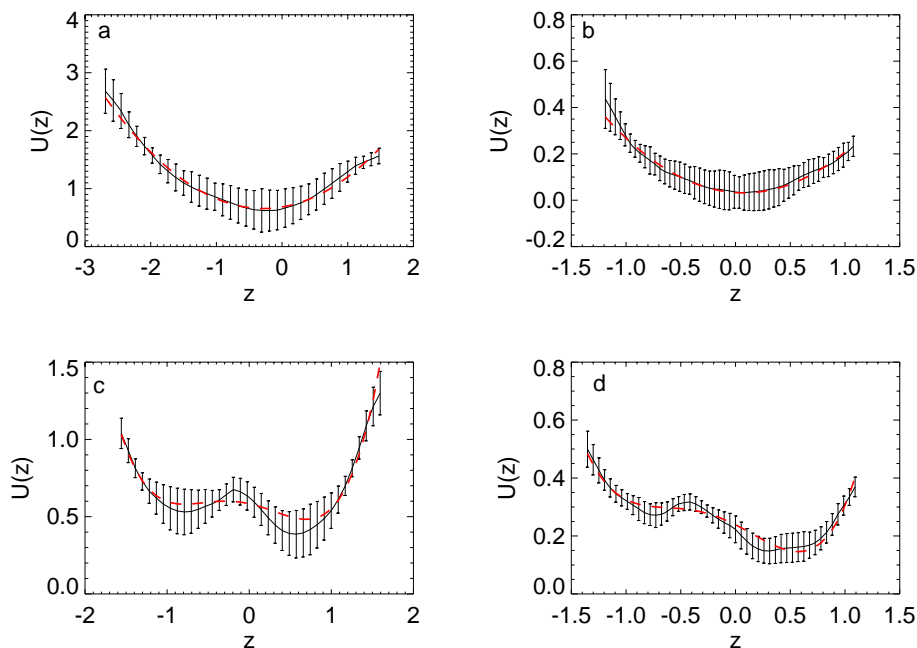Printer-friendly Version

Interactive Discussion

Fig. 6. Potentials $U(z)$ calculated from the data (black curves and error bars) using Eq. (11) and polynomial best fits (red dashed curves) for NGRIP reconstructions $N_H(t)$ **(a)**, $N_L(t)$ **(c)**, and EPICA reconstructions $S_H(t)$ **(b)**, $S_L(t)$ **(d)**.

Discussion Paper | Discussion Paper | Discussion Paper | Discussion Paper

CPD

10, 1129–1152, 2014

Fast temperature changes during the last glacial period

T. Alberti et al.

Title Page

Abstract | Introduction

Conclusions | References

Tables | Figures

|◄ | ►|

◄ | ►

Back | Close

Full Screen / Esc

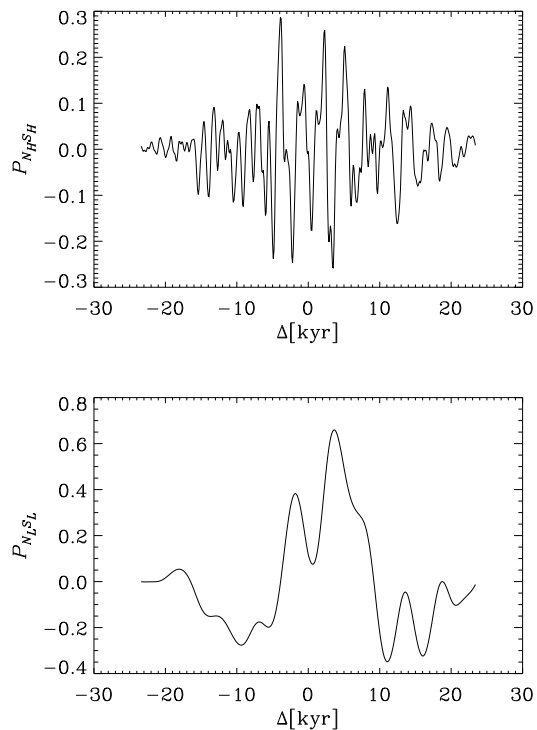Printer-friendly Version

Interactive Discussion

Fig. 7. Cross correlation coefficients between EPICA and NGRIP short time-scale ($P_{N_H S_H}(\Delta)$, top panel) and long time-scale ($P_{N_L S_L}(\Delta)$, bottom panel) EMD reconstructions.